LARGE EDDY SIMULATIONS OF SMOKE MOVEMENT IN THREE DIMENSIONS

by

Howard R. Baum, Kevin B. McGrattan,
and Ronald G. Rehm
Building and Fire Research Laboratory, and
Computing and Applied Mathematics Laboratory
National Institute of Standards and Technology
Gaithersburg, MD 20899

IN: Interflam '96. 7th International Interflam Conference, March 26-28, 1996, Cambridge, England. Proceedings. Sponsored by Interscience Communications Ltd., National Institute of Standards and Technology; Building Research Establishment; and Society of Fire Protection Engineers; and Swedish National Testing and Research Institute. Interscience Communications Ltd., London, England, Franks, C.A., and Grayson, S., Editors, 189-198 pp., 1996.

LARGE EDDY SIMULATIONS OF SMOKE MOVEMENT IN THREE DIMENSIONS

Howard R Baum, Kevin B McGrattan and Ronald G Rehm, National Institute for Standards and Technology, Gaithersburg, Maryland, USA

INTRODUCTION

This paper describes a methodology for simulating the transport of smoke and hot gases in enclosures. The approach is based on the use of efficient CFD techniques and high performance computers to solve a form of the Navier Stokes equations specialized to the smoke movement problem. The fire is prescribed in a manner consistent with a mixture fraction based approach to combustion, but the combustion phenomena themselves are not simulated. The mixing and transport of smoke and hot gases is calculated directly from an approximate form of the Navier Stokes equations. The computations are carried out as a three-dimensional time-dependent process, limited only by the spatial resolution of the underlying grid. No turbulence models are employed; the large scale eddies are simulated directly and sub-grid scale motions are suppressed. Present capabilities permit a typical residential room or hotel unit to be simulated at a 3-5 centimeter resolution limit, with correspondingly coarser resolution for larger spaces. The enclosure can have any shape made up of rectangular blocks, and can be multiply connected. The smoke is simulated by tracking a large number of Lagrangian elements, which originate in the fire. These same elements carry the heat released by the fire, providing a self consistent description of the smoke transport at all resolvable length and time scales. Large temperature and pressure variations are permitted, subject to the limitation that the Mach Number is much less than one. The next two sections give a brief description of the mathematical and computational aspects of the model, while the final section illustrates its capability with sample results and a comparison with experiment.

MATHEMATICAL MODEL

We consider a thermally expandable ideal gas driven by a prescribed heat source. The motion of the fluid is governed by the equations written in a form suitable for low Mach number applications[1]

$$\frac{\partial \rho}{\partial t} + \nabla \cdot \rho \mathbf{u} = 0 \tag{1}$$

$$\rho \left(\frac{\partial \mathbf{u}}{\partial t} + \frac{1}{2} \nabla |\mathbf{u}|^2 - \mathbf{u} \times \boldsymbol{\omega} \right) + \nabla p - \rho \mathbf{g} = \nabla \cdot \boldsymbol{\sigma} \tag{2}$$

$$\rho c_p \left(\frac{\partial T}{\partial t} + \mathbf{u} \cdot \nabla T \right) - \frac{dp_0}{dt} = \dot{q} + \nabla \cdot k \nabla T \tag{3}$$

$$p_0(t) = \rho \mathcal{R} T \tag{4}$$

Here, all symbols have their usual fluid dynamical meaning: ρ is the density, $\mathbf{u}$ the velocity vector, ω the vorticity, p the pressure, $\mathbf{g}$ the gravity vector, c_p the constant-pressure specific heat, T the temperature, k the thermal conductivity, t the time, $\dot{q}$ the prescribed volumetric heat release, $\mathcal{R}$ the gas constant equal to the difference of the specific heats $\mathcal{R} = c_p - c_v$, and σ the standard stress tensor for compressible fluids. Notice in the energy conservation equation that the spatially and temporally varying pressure has been replaced by an average pressure p_0 which depends only on time. This is done to filter out acoustic waves.

The divergence of the flow $\nabla \cdot \mathbf{u}$ is a very important quantity in the analysis to follow, and it is readily found by combining Eqs. (1) and (3) and using the equation of state (4)

$$p_0 \nabla \cdot \mathbf{u} + \frac{1}{\gamma}\frac{dp_0}{dt} = \frac{\gamma - 1}{\gamma}(\dot{q} + \nabla \cdot k\nabla T) \tag{5}$$

where $\gamma = c_p/c_v$. Integrating Eq. (5) over the entire domain Ω yields a consistency condition for the background pressure $p_0(t)$

$$p_0 \int_{\partial\Omega} \mathbf{u} \cdot d\mathbf{S} + \frac{V}{\gamma}\frac{dp_0}{dt} = \frac{\gamma - 1}{\gamma}\left(\int_\Omega \dot{q}\, dV + \int_{\partial\Omega} k\nabla T \cdot d\mathbf{S}\right) \tag{6}$$

where V is the volume of the enclosure. The background pressure can be expressed in terms of a background temperature $T_0(t)$ and density $\rho_0(t)$

$$p_0 = \mathcal{R}\rho_0 T_0 \tag{7}$$

These spatially averaged quantities play the same role that ambient conditions do in the Boussinesq approximation. Perturbations to each are represented by the relations

$$T = T_0(t)(1 + \tilde{T}) \quad ; \quad \rho = \rho_0(t)(1 + \tilde{\rho}) \tag{8}$$

The perturbation values are thus simply related

$$(1 + \tilde{T})(1 + \tilde{\rho}) = 1 \tag{9}$$

Defining T_0 and ρ_0 through the adiabatic process

$$\frac{\rho_0}{\rho_\infty} = \left(\frac{p_0}{p_\infty}\right)^{1/\gamma} \tag{10}$$

allows the energy equation to be expressed in terms of the perturbation temperature $\tilde{T}$ and the divergence

$$\frac{\partial \tilde{T}}{\partial t} + \mathbf{u} \cdot \nabla \tilde{T} = (1 + \tilde{T})\left[\nabla \cdot \mathbf{u} + \frac{1}{\gamma p_0}\frac{dp_0}{dt}\right] \tag{11}$$

The background pressure is found from Eq. (6).

Next, we simplify the momentum equation. The pressure is composed of three components, the background $p_0(t)$, the hydrostatic, and a perturbation to the hydrostatic $\tilde{p}$

$$p(\mathbf{r}, t) = p_0(t) - \rho_0(t) g z + \tilde{p}(\mathbf{r}, t) \tag{12}$$

where z is the vertical spatial component. We subtract off the hydrostatic pressure gradient from the momentum equation (2), and then divide by the density to obtain

$$\frac{\partial \mathbf{u}}{\partial t} + \frac{1}{2}\nabla|\mathbf{u}|^2 - \mathbf{u} \times \omega + \frac{1}{\rho}\nabla\tilde{p} - \frac{\rho - \rho_0}{\rho}\mathbf{g} = \frac{1}{\rho}\nabla \cdot \sigma \tag{13}$$

To simplify this equation further, the density in the pressure term is assumed ambient, and then the term $|\mathbf{u}|^2/2$ is combined with the perturbation pressure $\tilde{p}/\rho_0$ and written as a total pressure, $\mathcal{H}$. If the coefficient of viscosity is assumed constant, the momentum equation can be written

$$\frac{\partial \mathbf{u}}{\partial t} - \mathbf{u} \times \omega + \nabla\mathcal{H} + \tilde{T}\mathbf{g} = \nu\left(\frac{4}{3}\nabla(\nabla \cdot \mathbf{u}) - \nabla \times \omega\right) \tag{14}$$

For most applications, the effective kinematic viscosity coefficient ν represents dissipation on length scales below the resolution limits of the calculation. The effective Reynolds number is

high enough to permit direct simulation of convective motion over a spatial range of two orders of magnitude for a three-dimensional calculation.

In summary, the equations which are solved numerically are the energy equation (11), the momentum equation (14), and a Poisson equation for the total pressure, obtained by taking the divergence of Eq. (14). This linear elliptic equation is solved with the use of an FFT-based fast direct solver. The background pressure, temperature and density are found from Eqs. (6), (7) and (10). Each of the conservation equations emphasize the importance of the divergence and vorticity fields, as well as the close relationship between the thermally expandable fluid equations[1] and the Boussinesq equations for which the authors have developed highly efficient solution procedures[2,3]. These are applied directly to the equations presented here with minor modifications and no loss in performance. The only changes from earlier methodology are a return to a uniform rectangular grid with blocks of cells masked to simulate internal boundaries[8]; and the use of a second order Runge-Kutta scheme to advance the velocity and temperature fields in time. The speed and accuracy of this technique enable calculations on current generation workstations which involve over a million computational cells, yielding the spatial range of two orders of magnitude for a three-dimensional calculation.

THERMAL ELEMENTS

The fire is represented by introducing a large number of Lagrangian elements which release heat as they are convected about by the thermally induced motion. Since the fluid motion determines where the heat is actually released, and the heat release determines the motion, the large scale features of the coupling between the fire and the smoke transport are retained. It should be noted, however, that the heat release rate is *not* predicted, but is an input parameter in the computer programs implementing this model. The smoke is simulated by tracking the convected elements after the fuel burnout is completed. A specified percentage of the fuel consumed is assumed to be converted to smoke particulate. Thus, a knowledge of the spatial distribution of the Lagrangian elements is equivalent to a specification of the smoke particulate density at any instant of time.

The theoretical basis for the thermal element combustion model can be readily deduced from the mixture fraction representation of an isolated fire plume. Denoting this quantity by $Z(\mathbf{r},t)$, it is a solution to the equation:

$$\rho\left(\frac{\partial}{\partial t}+\mathbf{u}\cdot\nabla\right)Z=\nabla\cdot(\rho D\nabla Z) \tag{15}$$

The velocity vector $\mathbf{u}$ can always be decomposed into a solenoidal component $\mathbf{v}$ and an irrotational component $\nabla\phi$. The solenoidal component is by definition divergence free, while the potential flow carries the expansion of the gas induced by the combustion heat release. This follows from the mass conservation equation which can be written in the form:

$$\left(\frac{\partial}{\partial t}+\mathbf{u}\cdot\nabla\right)\rho+\rho\nabla\cdot\mathbf{u}=0 \tag{16}$$

Since by hypothesis $\rho=\rho(Z)$, combining equations (15) and (16) with the velocity decomposition described above yields the following equation for the potential function:

$$\nabla^2\phi=\frac{d(1/\rho)}{dZ}\nabla\cdot(\rho D\nabla Z) \tag{17}$$

Equation (17) clearly relates the potential flow to the mixture fraction and hence the combustion heat release. The next step is the assumption that the gasified fuel emerging from the condensed

phase is rapidly broken up into isolated deforming islands of reacting fuel surrounded by air. The mechanism controlling the breakup process is the local strain field generated by the fire. Under this assumption, the fire is a large collection of objects described and visualized by Baum *et al.*[4] In this view, each blob is carried along by the large scale motion and deformed by the local mixing which controls the combustion process in the blob.

The potential associated with each fuel blob can be expressed in terms of a modified mixture fraction $F(Z)$.

$$F(Z) = \frac{\int_0^Z \rho(Z) D(Z)\, dZ}{\int_0^1 \rho D\, dZ} \tag{18}$$

The specific volume $1/\rho$ is assumed to be a piecewise linear function of the mixture fraction on each side of the flame. Then two fuel-dependent constants K_+ and K_- can be defined, one for each side of the flame. They are:

$$K_+ = \frac{d(1/\rho)}{dZ} \int_0^1 \rho D\, dZ, \quad (Z < Z_{fl}) \tag{19}$$

$$K_- = \left|\frac{d(1/\rho)}{dZ}\right| \int_0^1 \rho D\, dZ, \quad (Z > Z_{fl}) \tag{20}$$

Here, Z_{fl} denotes the value of the mixture fraction at the flame sheet associated with the individual blob. Note that $Z > Z_{fl}$ inside the flame and $Z < Z_{fl}$ outside the blob. The solution for ϕ can now be written as:

$$\begin{aligned} \phi &= -K_- F(Z) + \phi_H, \quad (Z > Z_{fl}) \\ \phi &= +K_+ F(Z) + \phi_H, \quad (Z < Z_{fl}) \end{aligned} \tag{21}$$

$$\phi_H = \frac{1}{4\pi} \oint dS_{fl}\, \nabla F \cdot \mathbf{n}_{fl}\, \frac{(K_+ + K_-)}{|\mathbf{r} - \mathbf{r}_{fl}|} \tag{22}$$

The integral in Eq. (22) is taken over the flame surface, with $\mathbf{n}_{fl}$ denoting the outward pointing normal to the surface and $\mathbf{r}_{fl}$ a point on the flame.

The solution expressed by Eqs. (21) and (22) can be interpreted as follows. Each fuel containing element is convected in a large scale flow field described by:

$$\mathbf{u} = \mathbf{v} + \sum_n \nabla \phi_H(\mathbf{r} - \mathbf{r}_n, t) \tag{23}$$

Here, the sum is over the far field approximation to the expansion field induced by all the blobs, while $\mathbf{v}$ denotes the composite solenoidal velocity field. Writing $\phi_H(\mathbf{r} - \mathbf{r}_n, t)$ out explicitly:

$$\phi_H(\mathbf{r} - \mathbf{r}_n, t) = \frac{1}{4\pi |\mathbf{r} - \mathbf{r}_n|} \oint dS_{fl}\, \nabla F \cdot \mathbf{n}_{fl}\, (K_+ + K_-) \tag{24}$$

The quantity $\mathbf{r}_n$ is the centroid of the instantaneous surface of the flame sheet. Note that this is the solution corresponding to a point source of volume generated by the combustion heat release.

The precise location of $\mathbf{r}_n$ is irrelevant at scales much larger than the fuel blob. The important quantity in Eq. (24) is the integral which is proportional to the heat release associated with the blob. The direct calculation of this quantity would require the solution of the equations of motion including the mixture fraction down to length scales small enough to capture the local mixing and diffusion on the scale of the fuel element. This is not feasible at present, since

the active combustion zone of a fire is usually only a small fraction of the space that must be included in any simulation. This leaves two choices; either extract the equivalent information from a local model of the combustion processes at the scale of the fuel element (see Reference 4 for a preliminary calculation along these lines) or obtain the information empirically. In the present paper, the latter procedure is followed. The heat release rate $q_n(t)$ associated with the nth element is represented by a simple function with a time scale determined from the plume correlations summarized by Baum and McCaffrey[5]. Thus the heat release rate per unit volume in the energy equation (3) takes the form:

$$\dot{q} = \sum_n q_n(t)\,\delta(\mathbf{r} - \mathbf{r}_n(t)) \tag{25}$$

The thermal element model, which represents the combustion heat release as a large number of point sources convected by the resolvable flow field, is in fact a simple combustion model in its own right. It is consistent with more detailed combustion theories currently in use, and it permits the use of experimental data from fire experiments in a way that does not violate the consequences of those theories.

RESULTS

Four examples illustrating the present capabilities of the approach outlined are presented. First, an isolated pool fire simulated with the use of thermal elements is shown in Fig. 1. The figure depicts a 22 cm diameter pool fire with a 3 kW heat release rate. The domain simulated is 1.5 m on a side and 3 m in height. A computational mesh of $96 \times 96 \times 96$ cells is employed with the grid cells gradually stretched in the vertical direction. Three temperature contours are shown which correspond to the boundaries of the continuous flame, intermittent flame, and plume zones as defined in Baum and McCaffrey[5]. Note that Fig. 1 is an instantaneous snapshot of the fire, and that time averages of the output of this kind of simulation must be produced in order to make quantitative comparison with most experimental data. Indeed, it is the fact that the *results* of the simulation can be averaged in a routine way while the *equations* of fluid mechanics cannot is the basis of the whole approach presented here.

The next three calculations are of enclosure fire scenarios. First, a simulation of an enclosure fire experiment conducted by Steckler *et al.*[6,7] shows that reasonably good agreement with experimental results can be obtained at the levels of spatial resolution achievable with current CFD techniques and computer facilities. The overall geometry of the Steckler *et al.* experiments is shown in Fig. 2. The grid used was made up of $160 \times 96 \times 72$ cells roughly 3 cm on a side. The velocity vectors displayed in the vertical center plane after the flow has reached an apparent steady state are also shown. In addition to giving some idea of the overall flow pattern they give an indication of the spatial resolution achieved in the computation. The wireframe doorway velocity plot shows the characteristic orifice profile, with the maximum speed near the jet edge. This plot is remarkably similar to that given in Fig. 5 of Reference 6, where the experimental profiles are displayed. A quantitative comparison between theory and experiment is shown in Fig. 3, where time averaged doorway centerline velocity and temperature profiles are displayed. There are no adjustable parameters in the model, so the relatively good agreement between the measured and calculated results is an indicator of the *predictive* capability of the present approach.

Next, experiments conducted in a much larger enclosure are simulated to demonstrate that smoke movement in large spaces can be described with reasonably high resolution. In November 1994, NIST conducted smoke transport experiments in the FRI test facility in Japan. The

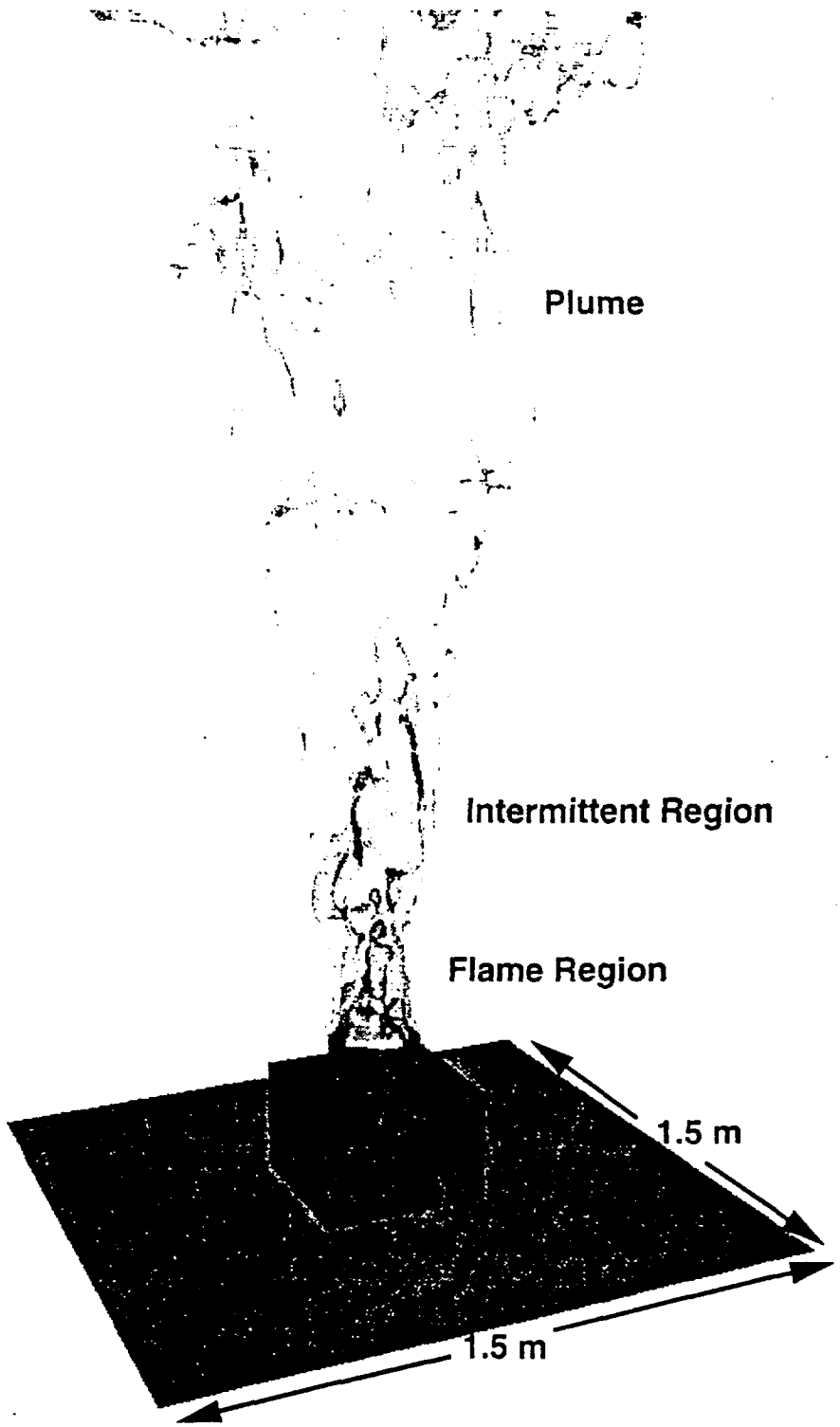

Figure 1: A simulation of a buoyant diffusion flame, showing the three major zones of the fire: the continuous flame, intermittent and plume regions.

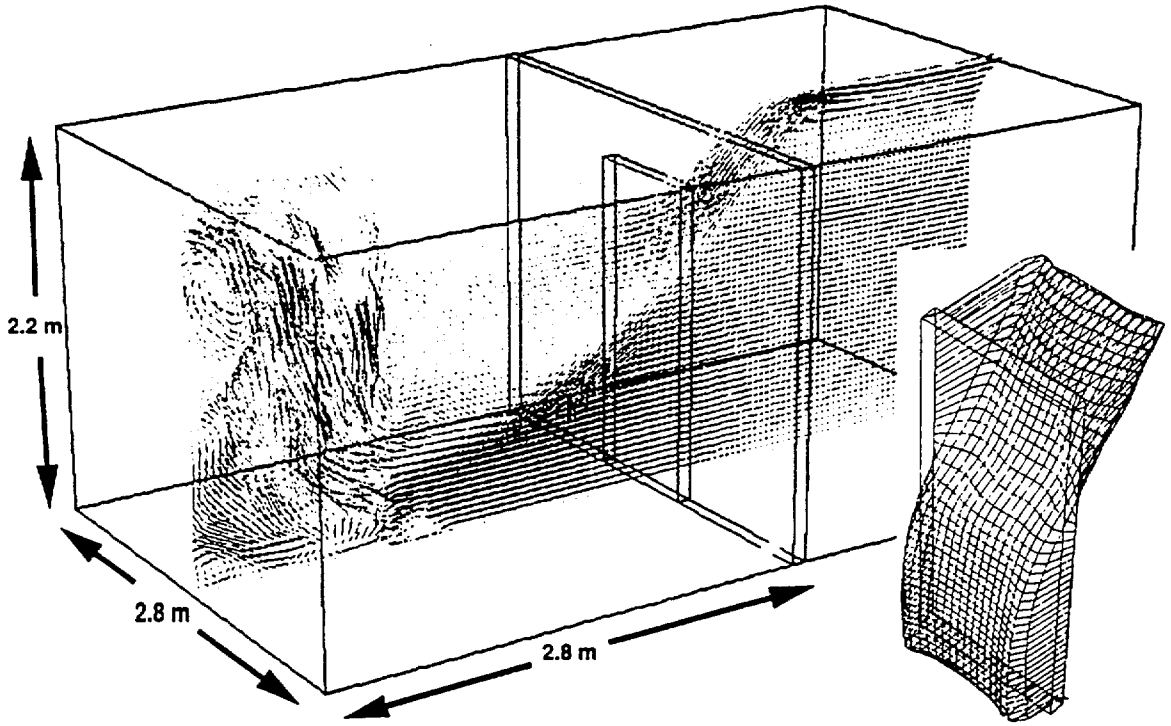

Figure 2: Geometry of Steckler *et al.* experiment, showing the velocity vectors along a slice down the centerline of the configuration. Shown at the right is the velocity profile in the doorway.

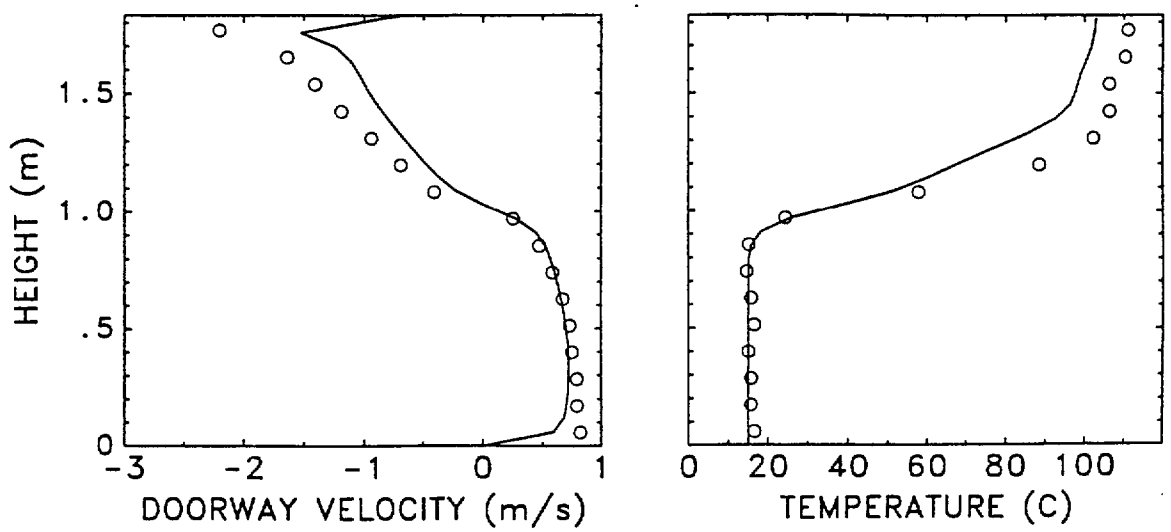

Figure 3: Comparison of experimental (circles) and simulation (lines) centerline temperature and velocity profiles in the doorway of the Stecker experiment.

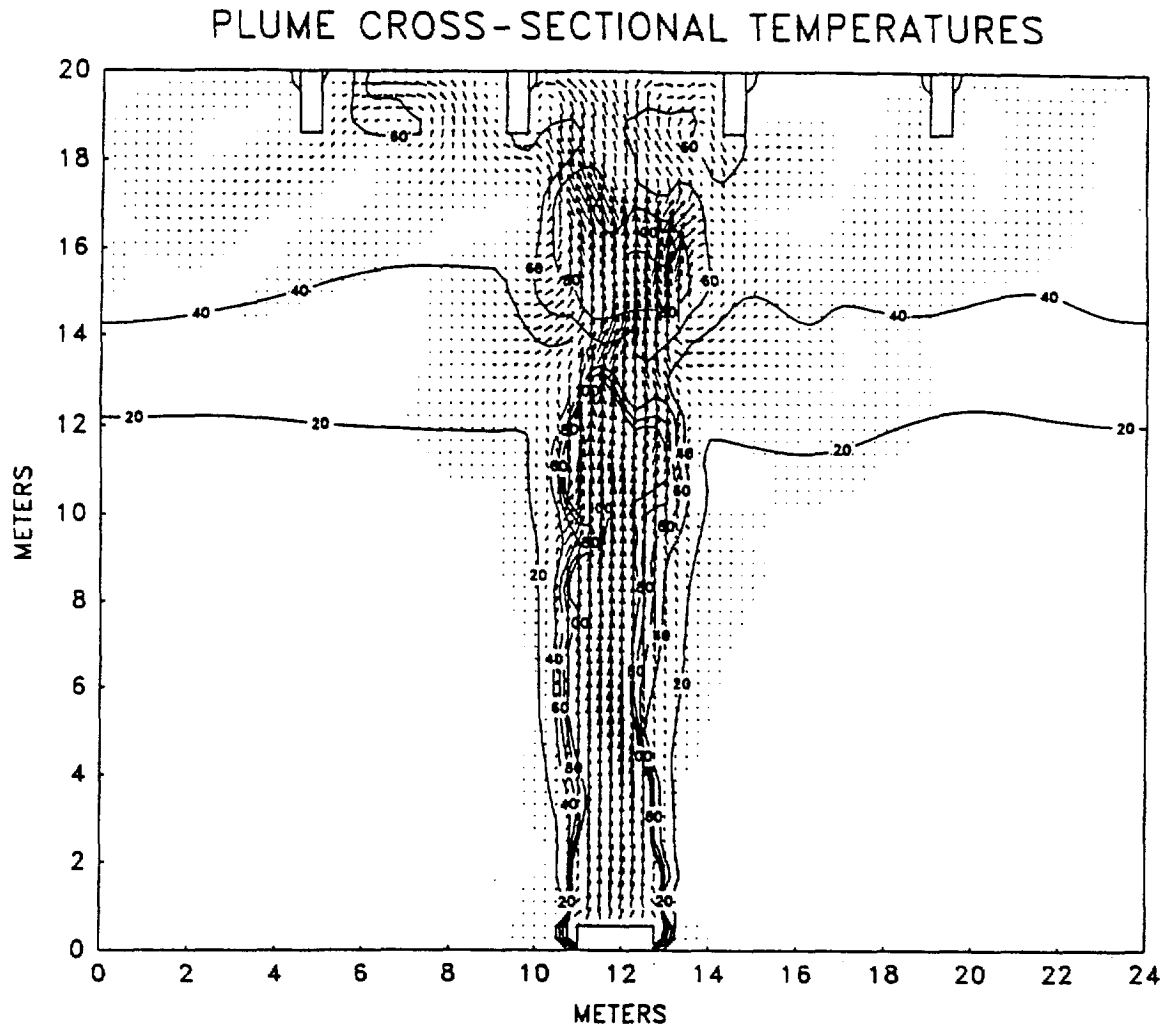

Figure 4: **Temperature and velocity vectors along the centerline plane of the FRI facility.**

building was 20 m tall and 24 m on each side, with large vents near the floor and ceiling for controlling the ventilation. A number of 1.2 m and 2 m pan fires with different fuels were studied. One of the tests, a 2 m, 5 MW heptane fire, was simulated using a spatial grid of $96 \times 96 \times 72$ cells to cover the entire facility. Figure 4 shows the temperature and velocity vectors in a slice down the center of the building. Thermocouples were placed directly above the fire, and recorded temperatures every second. Figure 5 shows the experimental and simulated time histories of the temperature during the burn. The time traces have not been averaged so as to indicate the large fluctuations that occur, and which are captured by the time-resolved calculations. Again, the explicit calculation of the large scale fluctuations distinguishes this approach from others which use empirical models in averaged equations.

Finally, a study of smoke movement induced by a fire in a hypothetical hotel unit demonstrates the level of geometrical complexity that can be simulated at present. The smoke plume from a fire on top of a bed in an idealized hotel room unit is shown in Fig. 6. The unit also contains a sofa to the right of the bed, as well as a chest of drawers and a desk on the opposite wall. A closet blocked off from the rest of the unit and a bathroom with open doorway are to the left. Air heated $10°C$ above ambient enters the room at 25 cm/sec through a duct on the lower right

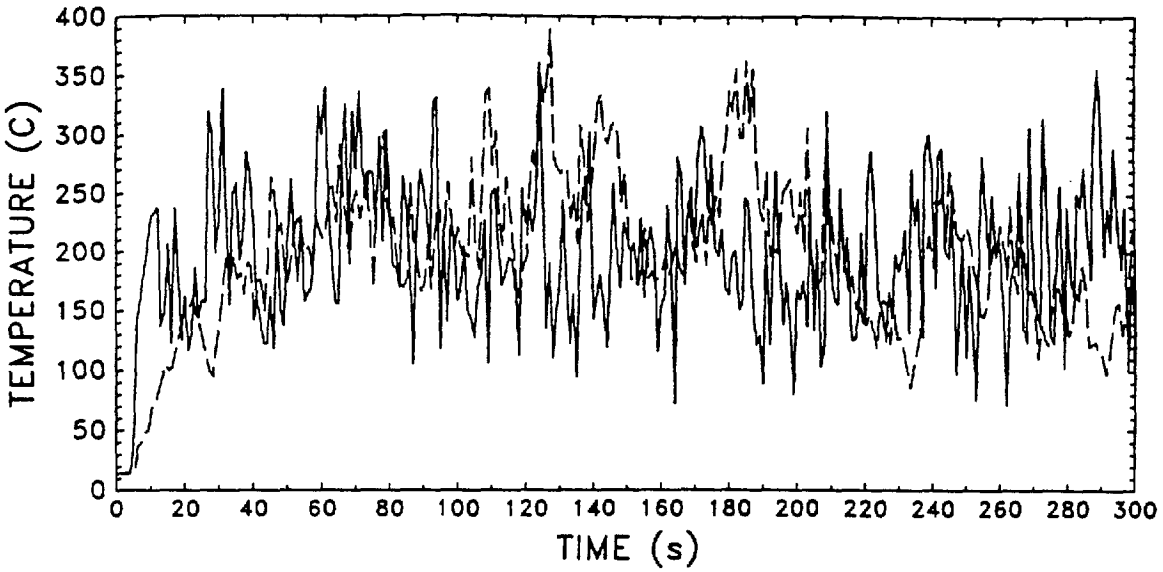

Figure 5: **Comparison of experimental (dotted line) and simulated temperature (solid line) time histories 9 m above a 5 MW heptane fire.**

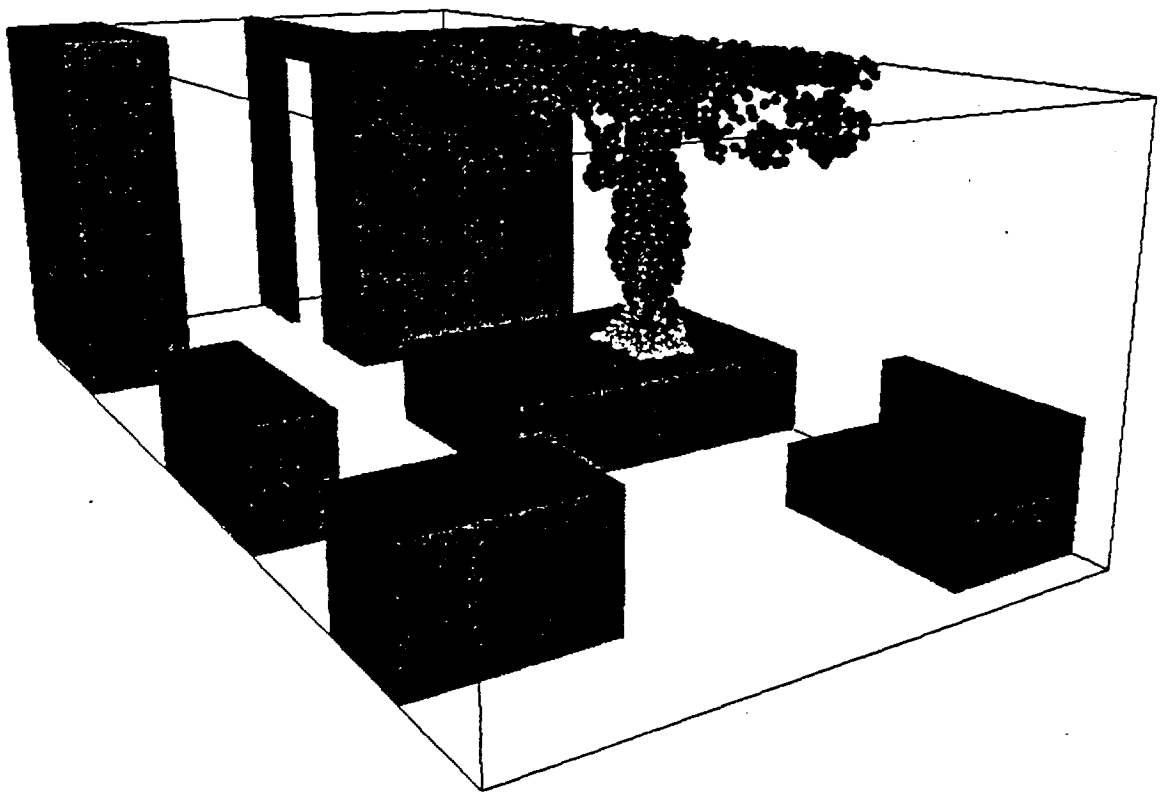

Figure 6: **Simulation of a hotel room fire, with ignition occurring on the bed. The dots represent thermal elements that originate at the bed.**

wall and is extracted on the upper left wall above a closed door with a 2 cm gap at the floor. The vents operate at fixed outside pressures, so the inflow is reduced and outflow increased as the room pressure rises due to the fire. The overall grid is composed of 192 × 96 × 64 4 cm cubes. The calculation simulates about one minute of real time. These computations required approximately 20 microseconds per cell per time step on an IBM RS 6000/58H server, and used 280 MBytes of memory.

CONCLUSION

These examples are intended to demonstrate that smoke movement caused by enclosure fires can be calculated with a rather high degree of accuracy directly from the underlying Navier Stokes equations in scenarios of practical interest. Although many other physical mechanisms need to be included before a full predictive capability is achieved, it is clear to us that the methodology outlined above is the only currently available way of *guaranteeing* increasingly accurate predictions of smoke movement in the future.

REFERENCE LIST

[1]RG Rehm and HR Baum, "The Equations of Motion for Thermally Driven, Buoyant Flows", *Journal of Research of the NBS*, Vol. 83, pp. 297-308, 1978.

[2]KB McGrattan, RG Rehm and HR Baum, "Fire Driven Flows in Enclosures", *Journal of Computational Physics*, Vol. 110, pp. 285-291, 1994.

[3]HR Baum, OA Ezekoye, KB McGrattan and RG Rehm, "Mathematical Modeling and Computer Simulation of Fire Phenomena", *Theoretical and Computational Fluid Dynamics*, Vol. 6, pp. 125-139, 1994.

[4]HR Baum, RG Rehm and JP Gore, "Transient Combustion in a Turbulent Eddy", *Twenty Third Symposium (international) on Combustion*, The Combustion Institute, Pittsburgh, pp. 715-722, 1990.

[5]HR Baum and BJ McCaffrey, "Fire Induced Flow Field - Theory and Experiment", *Fire Safety Science - Proceedings of the Second International Symposium*, pp. 129-148, Hemisphere, New York, 1989.

[6]KD Steckler, JQ Quintiere and WJ Rinkinen, "Flow Induced by a Fire in a Compartment", *Nineteenth Symposium (International) on Combustion*, The Combustion Institute, Pittsburgh, pp. 913-920, 1982.

[7]KD Steckler, HR Baum and JQ Quintiere, "Fire Induced Flows Through Room Openings - Flow Coefficients", *Twentieth Symposium (International) on Combustion*, The Combustion Institute, Pittsburgh, pp. 1591-1600, 1984.

[8]KB McGrattan "Low Speed Flows in Complex Domains", submitted to *Journal of Computational Physics*.